1

# Thermal Contraction of Aqueous Glycerol and Ethylene Glycol Solutions for Optimized Protein Crystal Cryoprotection

Authors

Chen Shen<sup>a</sup>, Ethan F. Julius<sup>a</sup>, Timothy J. Tyree<sup>a</sup>, David W. Moreau<sup>b</sup>, Hakan Atakisi<sup>b</sup> and Robert E. Thorne<sup>b</sup>\*

<sup>a</sup> Cornell University, Ithaca, NY, 14853

<sup>b</sup>Physics Department, Cornell University, Ithaca, NY, 14853, USA

Correspondence email: ret6@cornell.edu

**Synopsis** Measurements of the T=77 K glass-phase densities of drops with volumes down to 70 pL are used to determine the concentration-dependent thermal contraction of aqueous glycerol and ethylene glycol solutions. Application in optimizing cryocrystallographic outcomes by matching the contractions of external and internal solvent to those of the crystal and internal solvent spaces are discussed.

**Abstract** The thermal contraction of aqueous cryoprotectant solutions on cooling to cryogenic temperatures is of practical importance in protein cryocrystallography and in biological cryopreservation. In the former case, differential contraction on cooling of protein molecules and their lattice relative to that of the internal and surrounding solvent may lead to crystal damage and degradation of crystal diffraction properties. We have determined the amorphous phase densities of aqueous solutions of glycerol and ethylene glycol at T=77 K. Densities with accuracies of <0.5% to concentrations as low as 30% (w/v) were determined by rapidly cooling drops with volumes as small as 70 pL, assessing their optical clarity, and measuring their buoyancy in liquid nitrogen-argon solutions. Use of these densities in contraction matching of internal solvent to the available solvent spaces is complicated by several factors, most notably the exclusion of cryoprotectants from protein hydration shells and expected deviation of the contraction behaviour of hydration water from bulk water. The present methods and results will assist in developing rational approaches to cryoprotection and to an understanding of solvent behaviour in protein crystals.

Keywords: thermal expansion; aqueous solution; density; protein crystallography; cryocrystallography; cryopreservation; expansion matching; vitrification; vitreous; cryoflotation; buoyancy; partial specific volume

#### 1. Introduction

Roughly 98% of all protein structures have been determined using crystals cooled to T=100 K (Garman & Schneider, 1997; Garman, 1999; Garman & Doublié, 2003; Pflugrath, 2015). Cooling to cryogenic temperatures dramatically reduces the rate at which crystals are damaged by X-rays (Holton, 2009; Garman, 2010; Warkentin et al., 2013a), allowing more data to be collected per crystal, and reduces the contribution of thermal motions to atomic B factors, often giving modest increases in diffraction resolution. However, cooling also damages crystals. Crystal mosaicities – a measure of the distribution of lattice orientations within the crystal - always increase, from as-grown values of a few thousandth of a degree for well-ordered crystals (Fourme et al., 1995; Snell et al., 1995) to 0.2°-1° or more. This reduces the maximum achievable diffraction signal to noise and can lead to diffraction spot overlap, especially for e.g., viruses and large complexes, whose crystals have large unit cells. The distribution of lattice spacings within the crystal (and thus of spatial variations of lattice spacing) also increases, from <0.01% to 1% or more in unfavourable cases (Kriminski et al., 2002). All of these problems become worse if inadequate cryoprotection or too-slow cooling allow internal or external crystal solvent to crystallize on cooling. Crystalline ice contributes rings in the diffraction pattern that can interfere with protein lattice diffraction. Aside from degrading diffraction properties, cooling also introduces substantial crystal-to-crystal and even within-crystal nonisomorphism.

The mechanisms by which cooling increases protein crystal disorder are incompletely understood (Juers & Matthews, 2001, 2004a; b; Kriminski et al., 2002). Some disorder must result due to incomplete evolution of the protein's conformation toward its equilibrium configuration at each temperature as the crystal temperature drops, leading to a non-equilibrium conformation distribution and static disorder at 100 K (Halle, 2004; Keedy et al., 2014, 2015).

Excess solvent or oil surrounding a crystal will in general contract differently than the crystal on cooling. The resulting stresses may cause crystal bending and perhaps also cracking, especially for thin rod- and plate-shaped crystals.

Significant disorder may also result due to differences in contraction on cooling of protein molecules, the crystal unit cell, and the crystal's internal solvent (Juers & Matthews, 2001, 2004a; Kriminski et al., 2002; Alcorn & Juers, 2010). Protein crystals are composite materials, consisting of interpenetrating protein and solvent structures. Protein crystal unit cell volumes typically contract by 2-6% on cooling from 300 K to 100 K, and protein molecular volumes contract by 1-2% (Juers & Matthews, 2001, 2004a). The available unit cell volume for solvent then contracts by ~3-8%. However, when cooled into its glassy low-density amorphous (LDA) ice phase, pure bulk water actually expands on cooling from 298 K to 77 K by approximately 6% (Ghormley & Hochanadel, 1971; Debenedetti, 2003; Loerting et al., 2011), comparable to the net expansion that occurs when water is cooled to 77 K into its hexagonal ice phase (Röttger et al., 1994).

In general, as temperature decreases, the equilibrium amount of solvent within the unit cell will change, as the equilibrium volumes of solvent and of the crystal's solvent spaces change at different rates. If the crystal were cooled very slowly, solvent could in principle flow into or out of the crystal to maintain equilibrium. However, during rapid cooling in liquid nitrogen or  $100 \text{ K N}_2$  gas streams, long-range solvent transport from the crystal interior to its surface is impossible. Consequently, if there is an excess of solvent, it will tend to be pushed out of some crystal regions and to accumulate in others, leading to spatial variations in unit cell volumes and orientations and in formation of crystal defects needed to accommodate these variations. The increase in mosaicity and in the spread of unit cell parameters caused by cooling, as well as the breakup of crystals into mosaic domains visible in X-ray topography, are consistent with this mechanism (Kriminski et al., 2002). Solvent transport into and out of the crystal during transient warming from  $100 \text{ K to } \ge 273 \text{ K in part explains successful applications of cryoannealing (Juers & Matthews, 2001, 2004b).}$ 

An obvious remedy to these last two problems is to use a solution (or solutions) whose contraction on cooling matches that of the crystal and/or the solvent spaces in the crystal lattice (Juers & Matthews, 2001, 2004b; Kriminski et al., 2002; Alcorn & Juers, 2010). While pure water expands on cooling to 77 K, glycerol, ethylene glycol, and all other common cryoprotectants contract. By adjusting cryoprotectant type and concentration, it should in principle be possible to produce solutions whose contraction on cooling into the amorphous phase matches that of the solvent spaces within the protein lattice (Alcorn & Juers, 2010).

Unfortunately, the amorphous ice phase densities of common aqueous cryoprotectant solutions have only been measured at high cryoprotectant concentrations (Juers & Matthews, 2004b; Alcorn & Juers, 2010), typically 50% w/w and larger. At these large concentrations, the amorphous ice phase is readily obtained by cooling at slow rates (<10 K/s). Large volumes (>1 mL) and masses (≥1 g) can then be vitrified, and the solution density accurately determined by weighing cold samples in nitrogen gas and when immersed in liquid nitrogen. Solutions whose contraction matches that of protein crystals can be generated using such large cryoprotectant concentrations, but they may substantially perturb the protein's conformation and modify crystal packing.

Achieving the amorphous ice phase at lower cryoprotectant concentrations requires cooling rates that increase rapidly with decreasing concentration. For glycerol, ethylene glycol and several other common cryoprotectants, the critical cooling rate (CCR) to achieve amorphous ice varies according to CCR=CCR<sub>0</sub> exp(- $\beta$ c), where CCR<sub>0</sub> is the critical cooling rate of pure water and c is the solute concentration (Warkentin et al., 2013b). For glycerol solutions, critical cooling rates are <1 K/s at  $\geq$ 56% (w/v) (Sutton, 1991a; b),  $\sim$ 10 K/s at  $\sim$ 48% (w/v),  $\sim$ 100 K/s at  $\sim$ 36% (w/v),  $10^3$  K/s at  $\sim$ 27% (w/v), and increase to  $\sim$ 10<sup>6</sup> K/s for pure water. Cooling rates larger than  $\sim$ 10 K/s for three-dimensional (e.g., roughly spherical as opposed to thin-film) samples can only be achieved using sample volumes smaller

than  $\sim$ 1  $\mu$ l (Berejnov et al., 2006), corresponding to sample masses smaller than 1 mg. Ascertaining the density of such small masses by conventional buoyancy based measurements is impractical.

Here we report the amorphous phase densities of aqueous glycerol and ethylene glycol solutions to concentrations as low as 30% (w/v). We use microscope-based optical imaging to ascertain the phase (amorphous or crystalline) (McFerrin & Snell, 2002; Chinte et al., 2005; Berejnov et al., 2006; Meisburger et al., 2013) and a modified buoyancy based technique (Loerting et al., 2011) to measure the density of flash cooled drops with volumes as small as  $\sim$ 70 pL (masses as small as  $\sim$ 70 ng). These methods and results will assist in developing rational approaches to cryoprotection and to understanding solvent behaviour in protein crystals.

#### 2. Methods

Our initial attempts to measure the densities of individual drops of rapidly cooled cryoprotectant solutions below concentrations of ~50% (w/w), performed more than a decade ago, were based on determining the buoyant force on drops by weighing them, first when immersed in liquid  $N_2$  and second when in the cold gas immediately above the liquid  $N_2$  surface, as in the work of Alcorn and Juers (2010). To determine the weights of  $\mu$ L volume, milligram mass drops, a precision tensiometer with microgram resolution mounted on a mechanical isolation stage was used. The tensiometer and Dewar were shielded to eliminate air currents and baffles were inserted into the Dewar to damp out surface waves on the liquid nitrogen. In principle, this would have allowed weight measurements of 1  $\mu$ L (~1 mg) drops with ~0.2% accuracy, but hysteresis and drift in the tensiometer limited accuracy to 2% or worse. Cracking of 1  $\mu$ L and larger drops during cooling, which affects the displaced drop volume, was also common. Subsequent attempts to use a laser interferometer-based microbalance were also not successful.

The present method, based on cryoflotation (Loerting et al., 2011), does not require direct measurement of drop weights, but only a qualitative observation of their buoyancy, and so can yield highly accurate density measurements for drops of volumes down to the picoliter range.

Figure 1 shows the steps involved in a measurement. First, liquid drops are dispensed and then rapidly cooled using a liquid nitrogen/argon solution. Next, the drops are observed using a microscope to assess their state (crystalline or amorphous) and whether they are cracked. For each uncracked amorphous drop, lower-density liquid nitrogen is added as needed until the drop becomes neutrally buoyant. The density of the liquid nitrogen-argon mixture that yields neutral buoyancy is then determined by measuring the buoyant force on a 0.992 g test mass. This density then directly gives the density of the neutrally buoyant drop. Our experimental apparatus and protocol are described in detail below.

# 2.1. Cryoprotectant solutions

Aqueous solutions of glycerol and ethylene glycol (EG) were prepared at room temperature in 5% increments of w/v, the ratio of weight of cryoprotectant in grams (g) to total volume of solution in millilitres (mL), expressed in percent. Solutions were prepared by dispensing the desired mass of cryoprotectant (measured using a precision microbalance) into a test tube, adding water to bring the volume near 10 mL, and vortexing the mixture until it appeared optically uniform. Water was then added as needed to obtain a final volume of 10.0±0.1 mL, the solution vortexed, and its optical uniformity verified.

Concentrations in % (w/w), % (v/v), and in mole fraction are given by

$$C_{\%w/w} = \frac{C_{\%w/v}}{\rho_{solution}} , \qquad (1)$$

$$C_{\%v/v} = \frac{C_{\%w/v}}{\rho_{CVO}} , \qquad (2)$$

and

$$X_{\%} = \frac{100}{100 \frac{M_{cryo}}{M_{water}} \frac{1}{c_{\%w/w}} + \left(1 - \frac{M_{cryo}}{M_{water}}\right)},$$
 (3)

respectively. Here  $\rho_{solution}$  is the solution's density, previously determined at room temperature for aqueous solutions of glycerol (Bosart & Snoddy, 1928) and ethylene glycol (Rodrigues & Francesconi, 2011), and  $\rho_{cryo}$  is the density of pure cryoprotectant.  $M_{cryo}$  is the molar mass of cryoprotectant (92.09 g/mol for glycerol, 62.07 g/mol for ethylene glycol) and  $M_{water}$ =18.01 g/mol. Concentrations in % (w/v) and % (v/v) change with temperature as the solution volume changes, whereas concentrations in % (w/w) and mol % are independent of temperature. For this reason, % (w/w) is used here; results in % (w/v), more commonly used in cryocrystallography, are given in the Supporting Information. In units of % (w/v), pure water is 0% (w/v), pure glycerol is 126% (w/v), and pure EG is 111% (w/v).

#### 2.2. Coolant mixture generation and properties

Drops were cooled by projecting them onto or into a liquid nitrogen/argon solution. Liquid  $N_2$  boils at 77 K and liquid Ar freezes at 83.8 K. Direct mixing of the liquids leads to formation of argon slush. By slowly flowing Ar gas into liquid  $N_2$ , the Ar will disperse into the  $N_2$  to form a solution at 77 K. By adjusting the Ar concentration, the solution's density can be varied between those of liquid  $N_2$  (0.81 g/mL at 77 K) and Ar (1.4 g/mL at 84 K). This density range encompasses the low-temperature densities

of water (0.93 or 0.94 g/mL), glycerol (1.33 g/mL) (Blazhnov et al., 2004), and ethylene glycol (1.23 g/mL).

As shown in Figure 1(a), an inner copper container was suspended within a large glass Dewar flask. Initially, both the Dewar flask and the inner copper container were filled with pure liquid N<sub>2</sub> at 77 K. To generate an N<sub>2</sub>-Ar mixture, Ar gas was first precooled by flowing it through a coil suspended in the cold gas layer immediately above the Dewar's liquid N<sub>2</sub>, and then bubbled into the inner container's liquid. Precooling the Ar gas and using low Ar flow rates to minimize bubble formation reduced boil-off of liquid and consumption of Ar. The high thermal conductance of the inner container's copper walls ensured efficient transfer of latent heat from the condensing Ar to the surrounding liquid N<sub>2</sub>, minimizing boiling within the copper container, and ensured that the inner liquid's temperature remained at 77 K. Ar flow was continued until a desired solution density was obtained (~3 hours for a density of 1.3 g/mL), and then the tubing was removed. A mixer comprised of a thin horizontal copper plate with multiple pinholes attached to a vertical metal rod was used to mix the coolant solution and eliminate concentration and density gradients prior to each measurement. If Ar crystals appeared, a metal rod was used to mix the solution until they disappeared.

### 2.3. Drop generation and cooling

Drops were generated in two ways. A 1 mL syringe with a 33 gauge needle, combined with gentle tapping to release the drop from the tip, gave drop volumes down to  $\sim 1$  nL. In initial experiments using cryoprotectant concentrations down to 40% (w/v), drops descended  $\sim 14$  cm from the dispensing tip to the liquid N<sub>2</sub>-Ar surface. Dispensed drops would be briefly suspended above the N<sub>2</sub>-Ar surface on a cushion of vapour, during initial cooling in the film boiling regime. Most drop cooling thus occurred at the liquid surface and in the cold gas above it. This method could not generate the large cooling rates required to reliably vitrify drops with cryoprotectant concentrations below 40%.

As shown in Figure 1(b), for lower cryoprotectant concentrations, the cold gas layer above the liquid was gently removed just prior to plunging (Warkentin et al., 2006) using suction produced by a Venturi vacuum generator. Drops were dispensed using a 1 mL syringe with a 33 gauge needle onto a  $0.5 \times 1.5$  cm, 75  $\mu$ m thick polyester flag attached to a solid metal rod. The rod and flag were then plunged into the N<sub>2</sub>-Ar solution. When boiling ceased and cooling was complete, the solid drops were popped off the flag by gently flexing the flag using fine-tipped metal forceps. The suction was then stopped, and a cold gas layer allowed to reform above the liquid N<sub>2</sub>-Ar solution.

Drop volumes (diameters) used in these measurements ranged from a maximum of 1-4  $\mu$ L (~1-2 mm) for concentrations above ~70% that always formed amorphous phases, to ~2 nL (160  $\mu$ m) for intermediate cryoprotectant concentration drops (40-60 %w/v) dispensed directly into the N<sub>2</sub>-Ar solution, to ~70 pL (50  $\mu$ m) for low concentration drops dispensed on the polyester flags. In previous

cryoflotation measurements of pure hyperquenched glassy water (Loerting et al., 2011), the amorphous ice samples had volumes of roughly  $100~\mu L$  (masses of roughly 100~mg), and were prepared by vacuum cooling and deposition of roughly  $10^9$  - 5  $\mu m$  drops of pure water. Vacuum deposited samples generally contain voids and other defects that affect density measurements. Vacuum deposition of aqueous mixtures is challenging because evaporation may cause drop-size-dependent composition changes. By using individual drops, cracks and voids (bubbles) are easily eliminated by visual screening. Density determination of individual drops as small as 5  $\mu$ m may be possible, provided evaporation during dispensing and moisture condensation on cold drops are controlled, and provided drop observation times are extended to account for the smaller drop terminal speeds for a given density difference between the drop and the  $N_2$ -Ar mixture.

### 2.4. Assessing the state of the drop

As shown in Figure 1(c), the state of the drop after cooling was assessed by visual observation in a microscope. Drops that were optically clear were assumed to be vitrified, while those that were cloudy, milky, or opaque were assumed to be polycrystalline. This visual assay has been used in previous studies of drop vitrification (McFerrin & Snell, 2002; Chinte et al., 2005; Berejnov et al., 2006; Warkentin et al., 2013b), and correlates well with the absence or presence of ice rings in X-ray diffraction (Garman & Mitchell, 1996; Berejnov et al., 2006) and of excess low-q scatter in small angle X-ray scattering (SAXS) (Meisburger et al., 2013). Drops were lifted to just below the liquid surface, illuminated using a high intensity LED lamp, and observed using a boom-stand-mounted microscope. Cracked drops were removed from further consideration. Fogging and frosting due to condensation of moisture from the surrounding air was a serious problem during these observations, and was addressed as described in Section 2.6 below.

### 2.5. Measuring drop densities

The initial density of the  $N_2$ -Ar solution was adjusted to be somewhat above the expected density of the drops to be measured. Liquid  $N_2$  was added in volume increments beginning at 2 mL and decreasing to 0.25 mL until the drop became neutrally buoyant – as determined by perturbing the submerged drop using a rod and observing its motion through a microscope - or began to sink. Because the  $N_2$ -Ar solution tended to stratify into layers of different density, the solution was regularly mixed using the perforated horizontal copper plate. Surface tension did not affect measurements because  $N_2$ -Ar has a small surface tension and wets the drop surfaces, and because the neutral buoyancy condition was determined using fully submerged drops. As a check, floating drops were occasionally perturbed downward using either liquid  $N_2$  or a precooled metal rod to ensure that surface tension had been broken.

As shown in Figure 1(d), the density of the liquid  $N_2$ -Ar solution was measured by determining the apparent weight of a  $\sim$ 1 g,  $\sim$ 0.43 mL PTFE (Teflon) test mass when hanging in air at room temperature

 $(W_{t,air})$  and when submerged in the cryogenic solution at 77 K ( $W_{t,cryogen}$ ). The test mass was hung from the bottom of the pan of a precision microbalance (Mettler AE240) using 25  $\mu$ m diameter polymer line. Before submerging, the mass was precooled in liquid  $N_2$  to prevent boiling and changes in the concentration of the  $N_2$ -Ar solution. The test mass was then submerged roughly ½ of the depth of the liquid below the liquid's surface. This minimized effects of any density stratification that occurred after mixing and during measurements. Confining the liquid within the small-diameter copper container and efficient heat transfer through the container's walls to the liquid nitrogen outside eliminated boiling of the  $N_2$ -Ar solution and resulted in a highly quiescent liquid-gas interface, allowing the full resolution of the microbalance to be utilized. The change in buoyant force on the suspending line was estimated and found to be negligible compared with experimental uncertainties. Measurements at each cryoprotectant concentration were repeated at least twice to confirm buoyancy observations and density values.

From the apparent weights  $W_{t,air}$  and  $W_{t,cryogen}$ , the cryogen's density  $\rho_{cryogen}$  was calculated using Archimedes Principle as

$$\rho_{cryogen} = \frac{W_{t,air} - W_{t,cryogen} + \rho_{air} V_{t,298K} g}{V_{t,77K} g}$$
(4)

where  $\rho_{air} = 1.225$  g/L is the density of air at 298 K, and  $V_{t,298K}$  and  $V_{t,77K}$  are the volumes of the test mass at 298 K and 77 K, respectively. (Since the microbalance reports "weight" in grams, the factor g=9.81 m/s<sup>2</sup> is automatically included in its measurements.)

The volume  $V_{t,298K}$  of the PTFE test mass at room temperature was determined, first, by measuring its apparent weight in air and in isopropyl alcohol, and second, by measuring its dimensions using a precision calliper and (for the through-hole by which it was suspended) calibrated steel rods. The test mass volume at 77 K,  $V_{t,77K}$ , was determined by measuring the mass's apparent weight in liquid nitrogen.

When examining vitrified drops of aqueous cryoprotectant solutions, it was very difficult and time consuming to obtain precisely the right  $N_2$ -Ar solution composition to achieve perfect neutral buoyancy. So in most cases, the minimum solution density at which the drop clearly floated and the maximum density at which it clearly sank were determined, with the difference between these densities made as small as practical. The density of each drop was then estimated as the arithmetic mean of these values.

The primary source of uncertainty in the drop density measurements was the difference between the floating and sinking densities, typically 0.3%. Mass measurements were accurate to  $\pm 0.05$  mg or <0.01% of the test mass. Uncertainty in the density of liquid nitrogen was <0.1%, and uncertainty in

the density of the  $N_2$ -Ar solution due to imperfect mixing, density stratification, and evaporation of  $N_2$  or Ar between drop and test mass measurements was <0.5%, estimated from the repeatability of measurements. Uncertainty in drop concentrations of glycerol or ethylene glycol due to mixing errors and evaporation were <1%.

### 2.6. Low humidity environment

Condensation of water and ice formation caused significant difficulties. Condensation on the drop, the test mass, and suspending line all caused weight measurement errors. Condensation in the cold gas above the liquid nitrogen/argon solution caused fogging that it made it difficult to visualize and assess the state of the drop. Condensation leading to ice in the liquid  $N_2$ -Ar reduced visibility as drops descended and ascended through it, and made tracking of individual drops difficult. To minimize these effects, the measurements were performed in a low humidity environment. The experiment was contained in an acrylic (PMMA) and polyethylene sheet enclosed workbench, into which dry (<1% r.h.) room-temperature air flowed. All exposed cold Dewar, copper container, and liquid cryogen surfaces were covered by foam insulation. A  $\sim$ 1 inch diameter hole in a top foam disk, covered by a plastic flapper valve, provided access to drops in the copper container. A small flow of dry  $N_2$  gas into the space between the liquid and the foam (Figs. 1(a)-(d)) ensured that there was sufficient overpressure at all times to prevent ambient air flow into the Dewar. Gloves and masks were worn during sample manipulation and measurements to reduce moisture release and minimize perturbing air flows.

# 3. Results

Figure 2 shows the densities of (a) glycerol-water and (b) ethylene-glycol water solutions versus cryoprotectant concentration in % (w/w), as determined here at 77 K and as determined in previous measurements (Bosart & Snoddy, 1928; Rodrigues & Francesconi, 2011) at room temperature. Plots vs. concentration in % (w/v) are given in Figure S1. The density point at 0% concentration of 0.94 g/ mL is the currently accepted 77 K density for low-density amorphous (LDA) ice, the expected phase of pure amorphous water formed at atmospheric pressure (Debenedetti, 2003; Loerting et al., 2011). For both glycerol and ethylene glycol, extrapolation of our measured 77 K data to zero concentration appears to be consistent with this density. Interpolated densities at 50% (w/w) of 1.187(5) and 1.144(5) mg/mL for ~2 nl drops of glycerol-water and ethylene glycol-water solutions are consistent with values of 1.181(2) and 1.139(2) measured by Alcorn and Juers using ~0.7 mL samples. Cooling rates for our samples, with volumes ~10<sup>3</sup> to 10<sup>5</sup> times smaller, were much larger than those of Alcorn and Juers. The slightly higher densities measured here are consistent with a smaller fraction of microcrystalline ice (which has a lower density) expected with faster cooling. On the other hand, the very small density differences — comparable to experimental uncertainties — indicate that the density (and thus the structure) of the low-temperature amorphous phase does not depend appreciably on cooling rate, at least

in the cooling rate range explored. At 298 K, the density varies roughly linearly with cryoprotectant concentration for both glycerol and (less accurately) for ethylene glycol. At 77 K, the density at first increases rapidly with cryoprotectant concentration, and then beyond ~50% w/w increases much more slowly.

In the study of volumetric properties of liquid mixtures, it is more common to plot the excess specific volume  $v^E$  (in mL/g) (or excess molar volume in L/mole,  $\tilde{v}^E$ ) of the solution, which is defined as the difference between the actual solution specific volume

$$v_{actual}\left(c_{\%w/w}, T\right) = \frac{V_{actual}\left(T\right)}{m_{cryo} + m_{water}} = \frac{1}{\rho_{solution}\left(c_{\%w/w}, T\right)} \tag{5}$$

and its "ideal" value,

$$v_{ideal}\left(c_{\%w/w},T\right) = \frac{1}{m_{cryo} + m_{water}} \left(\frac{m_{cryo}}{\rho_{cryo}\left(T\right)} + \frac{m_{water}}{\rho_{water}\left(T\right)}\right)$$

$$= \frac{\frac{c_{\%w/w}}{100}}{\rho_{cryo}\left(T\right)} + \frac{1 - \frac{c_{\%w/w}}{100}}{\rho_{water}\left(T\right)}$$
(6)

where  $m_{cryo}$  and  $m_{water}$  are the masses of the solution's components. The "ideal" value assumes that the specific volumes of cryoprotectant and water in the solution are the same as they are in their pure bulk forms. The excess specific volume can be written as

$$v^{E}(c_{\%w/w}, T) = \frac{1}{\rho_{solution}(c_{\%w/w}, T)} - \left(\frac{\frac{c_{\%w/w}}{100}}{\rho_{cryo}(T)} + \frac{1 - \frac{c_{\%w/w}}{100}}{\rho_{water}(T)}\right).$$
(7)

This is plotted for glycerol and ethylene glycol at 77 K and 298 K vs.  $c_{\%w/w}$  in Figure 3 and vs.  $c_{\%w/v}$  in Figure 82. At room temperature, the deviation of the actual specific volume from its ideal linear behaviour is small at all concentrations. Deviations from linearity at 77 K are much larger. The excess specific volume has a maximum value near 50% w/w of ~-0.065 mL/g, or roughly 7% of the total specific volume for both glycerol and ethylene glycol, compared with ~1% at 298 K.

The solid line fits in Figures 3 and S2 have the form

$$v_{fit}^{E}(c_{\%w/w},T) = a_{0}(T) \exp \left[ -\frac{\left(\frac{c_{\%w/w}}{100} - a_{1}(T)\right)^{2}}{2a_{2}^{2}(T)} \right] + a_{3}(T), \quad (8)$$

where  $a_0$ ,  $a_1$ ,  $a_2$ , and  $a_3$  are coefficients given in Table S1, found by nonlinear regression to the data. There are no theoretical predictions for the amorphous densities of aqueous cryoprotectant solutions, and the functional form of these fits is motivated by the shape of the excess specific volume curves in Fig. 3. The solid line fits in Figures 2 and S1 are given by

$$\rho_{fit}\left(c_{\%w/w},T\right) = \frac{1}{v_{ideal} + v_{fit}^{E}}, \qquad (9)$$

where the first term in the denominator is the straight line given by Eq. 6 and the second is given by the fit of Eq. 8.

Figure 4 shows the experimental fractional change in specific volume between room temperature and 77 K,  $100\% \times \left[v(77 \text{ K}) - v(298 \text{ K})\right]/v(298 \text{ K})$ , as a function of concentration for glycerol and ethylene glycol, and fits given by the difference between the 298 K and 77 K fits in Figure 2. The largest thermal contractions are  $\sim 6.5\%$  for glycerol concentrations between  $\sim 60\%$  and 80%, and  $\sim 9.5\%$  for pure EG. The solution contractions remain close to those of the pure cryoprotectants down to  $\sim 60\%$  (w/w). From the fits, the crossover between thermal expansion on cooling at low concentrations and thermal contraction at high concentrations occurs at  $\sim 23\%$  (w/w) (21% (w/v)) for glycerol and  $\sim 19\%$  (w/w) (17% (w/v)) for ethylene glycol. The data for glycerol at concentrations of 50% and above are in general agreement with those previously reported (Juers & Matthews, 2004b; Alcorn & Juers, 2010).

#### 4. Discussion

### 4.1. Concentration dependence of density in aqueous glasses

For binary liquid mixtures, deviations of the specific volume from the "ideal" linear behaviour described by Equation 6, connecting the pure phases of the two liquids, are typically discussed in terms of attractive or repulsive interactions between the two molecular constituents and/or changes in locally ordered structures within the liquid (Egorov et al., 2010; Egorov & Makarov, 2014).

For aqueous glasses, deviation from the high cryoprotectant concentration linear asymptote to the specific volume, shown in Figure 5, rather than deviation from a line between the specific volumes of pure water and pure cryoprotectant, may reflect the most important physics. The 9% increase in specific volume that occurs when liquid water transforms to hexagonal ice at 273 K is due to the formation of a relatively open tetrahedral network that "expels" interstitial waters present in the liquid phase, resulting in less dense packing. On cooling below the phase transition temperature, hexagonal ice contracts like any normal solid, and its specific volume decreases to 1.072 mL/g at 77 K (Loerting et al., 2011). Low-density amorphous (LDA) ice has a density of ~1.067 mL/g at 77 K (Loerting et al., 2011), comparable to that of hexagonal ice. Experiments and simulations suggest that it, too, has an average oxygen coordination number near four, and a local, open structure that is similar to that of crystalline ice (Debenedetti, 2003).

Cryoprotectants inhibit the formation of this open structure on cooling. Our data suggest that at low cryoprotectant concentrations, each added cryoprotectant molecule disrupts water's local tetrahedral order and has a relatively large effect on the amorphous phase structure, so that the decrease in specific volume is relatively rapid. At high concentrations of glass-formers like glycerol and ethylene glycol, the amorphous structure is dominated by their respective disordered hydrogen bonding networks, in which the water molecules are a guest. Adding water increases hydrogen bonding between glycerol and water but does not disrupt a low-density structure like that which forms in pure water. The change in density with cryoprotectant concentration at high concentrations should thus be roughly linear, until the concentration drops to the point that the fraction of waters involved in open tetrahedral networks becomes substantial.

A sense of the differences in glass structure in the low and high cryoprotectant concentration regimes can be obtained by calculating the apparent specific volumes  $v_{cryo}^{app}\left(c_{\%w/w}\right)$  of the cryoprotectants, assuming that the water has the same specific volume at all cryoprotectant concentrations as it does in pure LDA ice. These can be calculated as

$$v_{cryo}^{app}\left(c_{\%w/w}\right) = v_{solution} + \left(\frac{100}{c_{\%w/w}} - 1\right)\left(v_{solution} - v_{water}^{0}\right), \tag{10}$$

and are plotted in Figure 6(a). For both glycerol and ethylene glycol, the apparent specific volumes at 30% (w/w) are roughly 77% of their values in their pure amorphous phases ( $c_{\%w/w} \rightarrow 100\%$ ), presumably because cryoprotectant molecules added to pure water disrupt the local water structure so as to decrease water's local specific volume below that in pure LDA ice.

Similarly, the apparent specific volume of water in cryoprotectant can be calculated, assuming that the cryoprotectant has the same specific volume at all water concentrations as it does in the pure cryoprotectant, as

$$v_{water}^{app}\left(c_{\%w/w}\right) = v_{solution} + \frac{c_{\%w/w}}{100} \left(\frac{1}{1 - \frac{c_{\%w/w}}{100}}\right) \left(v_{solution} - v_{cryo}^{0}\right). \tag{11}$$

This is plotted versus cryoprotectant concentration in Figure 6(b). Water's concentration-dependent apparent specific volume is the same (to within experimental uncertainties<sup>1</sup>) for both glycerol and ethylene glycol. In the dilute limit  $c_{\%w/w} \rightarrow 100\%$ , where water's tetrahedral network is absent,  $v_{water}^{app}\left(c_{\%w/w}\right) \sim 0.896$  mL/g (which can be obtained from the zero concentration intercepts of the high

<sup>&</sup>lt;sup>1</sup> Small errors in specific volume of the solution give large errors in the apparent specific volume of water as the water concentration approaches zero; the data points in this limit are currently being remeasured to improve their accuracy, and will be updated in the final version of the figure.

concentration asymptotes in Fig. 5). This is 15.6% smaller than that of pure LDA ice. It is  $\sim$ 5% larger than the specific volume 0.855 mL/g of high density amorphous (HDA) ice, where water molecules fill interstitial sites within the tetrahedral network (Bowron et al., 2006). Perhaps coincidentally, extrapolating a linear asymptote to the temperature-dependent density of liquid water as it approaches its boiling point at 373 K (where the tetrahedral network is also disrupted) down to 77 K gives a specific volume of  $\sim$ 0.87 mL/g.

# 4.2. Metrics for cryoprotectant effectiveness

Metrics commonly used to assess the effectiveness of cryoprotectants include suppression of the melting point (especially relevant to slow cooling protocols used in, e.g., cell cryopreservation and in calorimetric studies) and reduction of the critical (minimum) cooling rate required to obtain vitreous ice (relevant to fast cooling / vitrification protocols) versus cryoprotectant concentration in % (w/w). The change in solution specific volume between, e.g., room temperature and 77 K, for cryoprotectants at equal concentration in % (w/w), provides a metric relevant to thermal contraction matching of cryosolutions (Alcorn & Juers, 2010). Concentration in % (w/w) rather than mol% is generally most useful; it normalizes to some extent the differences in molecular size, and facilitates comparison of e.g., different molecular weights of polymers like polyethylene glycol on a per monomer basis.

The present measurements suggest the disruption of the open tetrahedral network of LDA ice, which leads to the initial rapid decrease in specific volume with cryoprotectant concentration at small  $c_{WW/W}$ , as a salient feature. Possible metrics include the initial slope S of specific volume vs. cryoprotectant concentration, normalized by the specific volume difference between pure LDA ice and pure cryoprotectant,

$$S = -\frac{100}{\left(v_{LDA\,ice}^0 - v_{cryo}^0\right)} \frac{\partial v}{\partial c_{\%w/w}} , \qquad (12)$$

or the intersection concentration  $c_{\%w/w}^{int}$  of linear fits to the low- and high-cryoprotectant concentration regimes, as shown in Figure 5. For glycerol and ethylene glycol, S is 1.58 and 1.72 and  $c_{\%w/w}^{int}$  is 49.4% (w/w) and 47.8% (w/w), respectively.

### 4.3. Thermal contraction matching in protein cryocrystallography

The possible consequences of thermal contraction mismatch and the potential benefits of contraction matching have been discussed previously (Juers & Matthews, 2001; Kriminski et al., 2002), most recently and thoroughly by Alcorn and Juers (Alcorn & Juers, 2010). Thermal contraction matching divides into (at least) two problems.

# 4.3.1. Contraction matching the crystal

The first problem is to match the contraction of the material *outside* the crystal to the contraction of the crystal. Loop-mounted crystals are typically surrounded by many times their own volume of mother liquor, cryoprotectant solution, or oil. Differences in contraction between this material and the crystal will generate stresses that cause crystal bending, cracking, and mosaicity increase, especially for crystals with rod- or plate-like morphologies or fragile lattices. Because both room temperature and low temperature cell parameters have rarely been measured for identically-prepared crystals with identical cryoprotectant concentrations, available cell contraction data are extremely limited. Data in Juers and Matthews (2001) suggest an average unit cell volume contraction  $\Delta V_{cell}$  near 4% with a range between roughly 2% and 6%. From Figure 4, matching these contractions using glycerol (ethylene glycol) requires concentrations between ~33% and 56% (w/w) (27 and 43% (w/w)). These are large compared with concentrations typically used in crystallization solutions and cryoprotectant soaks. They could affect protein conformation if used in growth solutions, and could cause crystal cracking if used for post-growth soaks unless the "soak" duration were limited to a few second "swipe" prior to plunge cooling. Data of Alcorn and Juers (2010) at 50% (w/w) indicates that high molecular weight PEGs, DMSO, and MPD contract 25% more than ethylene glycol and so could be more appropriate. The largest contractions at 50% (w/w) - roughly double that of ethylene glycol - are achieved with 2propanol, methanol, and ethanol, but these are the most perturbing of protein conformation. Alcohols are also highly volatile, requiring careful handling to ensure concentrations are maintained through to plunge cooling.

#### 4.3.2. Contraction matching internal solvent spaces

The second problem is to match the contraction of the solvent *inside* the crystal to that of the protein and lattice. On cooling, the unit cell volume  $V_{\text{cell}}$  shrinks, as does the volume  $V_{\text{protein}}$  of the protein molecules within the cell (Juers & Matthews, 2001; Alcorn & Juers, 2010). The volume within the cell available to solvent changes by  $\Delta V = \Delta V_{cell} - \Delta V_{protein}$ , and dividing by the room temperature solvent channel volume gives its fractional change. Using typical values of  $\Delta V_{cell} / V_{cell}^{RT} = -0.042$ ,  $\Delta V_{protein} / V_{protein}^{RT} = -0.013$ , and a protein volume fraction  $v_{prot} = 0.47$ , Alcorn and Juers estimated that typical proteins would require an ethylene glycol concentration of ~50% (w/w) (~55% w/v). Kriminski *et al.* (2002) estimated the density of flash-cooled glycerol-water mixtures by simple linear interpolation between the densities of LDA ice and amorphous glycerol, assumed that the glycerol-to-water ratio in the crystal is the same as in the soak or growth solution, ignored the differential contraction of the cell and protein, and ignored water inside the first hydration shell, and estimated the contraction matching glycerol concentration for tetragonal lysozyme to be ~28% (w/w) (~30% (w/v)).

However, several complications make contraction matching of internal solvent less than straightforward. First, the cooling-induced unit cell contraction determined by crystallography likely

differs from the actual contraction of the crystal, because cooling also produces a large increase in crystal disorder, as reflected in large increases in crystal mosaicity and in the spread of unit cell parameters. For example, if excess solvent is expelled from some crystal regions that remain ordered and accumulates in disordered/disrupted regions, the X-ray determined cell volume will be dominated by the ordered regions, and will overestimate the contraction of the crystal as a whole (Kriminski et al., 2002).

Second, the actual concentration of cryoprotectant within the crystal will be different than in the growth or soaking solution. In general, the chemical potential of solutes within a crystal will be different than in the surrounding bulk solution, leading to differences in concentration on a per unit volume or per protein molecule basis. For example, salt (Vekilov et al., 1996; Kmetko et al., 2006) and impurity protein (Caylor et al., 1999; Malkin & Thorne, 2004) concentrations within protein crystals are different than in the mother liquor from which they grow, on a per volume and per protein molecule basis. For common cryoprotectants, an extreme example is provided by large molecular weight PEGs, which have difficulty penetrating into all but the largest channels and cavities within protein lattices.

Third, the cryoprotectant concentration within protein hydration shells is generally much smaller than in bulk solution for proteins in solution, and this must also be true for proteins in crystals. A wide variety of compounds including sugars, polyols, amino acids, methylamines, and inorganic salts, encompassing glycerol, ethylene glycol, and many other compounds routinely used as cryoprotectants in cryocrystallography and in cryoprotection of proteins in solution, have been shown to be preferentially excluded from globular protein surfaces. In their presence, protein surfaces are preferentially hydrated (Timasheff, 1993, 2002; Parsegian et al., 2000; Shimizu & Smith, 2004; Sinibaldi et al., 2007), and this has a stabilizing effect on protein structure. Monohydric alcohols including methanol and ethanol are an exception: they preferentially bind at protein surfaces (Sinibaldi et al., 2007), contributing to their destabilizing effect on protein structure. Crystallographic studies of tetragonal and monoclinic lysozyme at room temperature (Datta et al., 2001; Saraswathi et al., 2002) found that the addition of sucrose, sorbitol, and trehalose to the mother liquor had essentially no effect on the number of detected hydration waters relative to the cryoprotectant-free structures. Crystallographic study of thaumatin crystals at 100 K grown with and without 31% (w/v) glycerol showed that waters within the first hydration shell were largely unaffected by the glycerol; the glycerol-free structure did have more modelled waters in the second shell, although these had higher B factors (Charron et al., 2002). Differences in second hydration shell water counts could simply reflect differences in the extent to which that shell is ordered, rather than the presence of glycerol within the shell.

Finally, the thermal expansion behaviour of solvent within the hydration shells may differ substantially from those of bulk solutions, both due to differences in cryoprotectant concentration and due to differences in their structure owing to water interaction with the protein surface. Water's density within the first hydration shell is ~15% larger than in bulk water due to a geometric effect and due to structural

changes (Merzel & Smith, 2002). Its thermal contraction behaviour might be expected to more closely match that of the protein itself.

These last three effects thus render the thermal expansion behaviour of water within the first two hydration shells uncertain. Any effects of cryoprotectants upon hydration shell expansion are also uncertain, but are likely to be much less than in bulk solvent. This suggests that the potential benefits of choosing cryoprotectants based on their expansion behaviour will be greatest for crystals with large solvent contents and large solvent channels, and that benefits for low solvent content crystals may be modest at best.

#### 5. Conclusion

Here we have demonstrated a robust experimental method, based on Archimedes Principle and cryoflotation (Loerting et al., 2011), for determining the amorphous phase densities and thermal contractions of aqueous cryoprotectant solutions using nanoliter to picoliter volume drops. Straightforward improvements to our methods should allow drop vitrification and measurement down to cryoprotectant concentrations of 15% (w/w), far lower than has previously been possible, and the mapping of amorphous phase densities for a wide variety of aqueous systems. These methods can be applied to determine partial specific volumes of protein within aqueous glasses, and so may yield information about cooling-induced changes in protein hydration and structure relevant both to cryocrystallography and to cryoSAXS (Meisburger et al., 2013).

The present results should be directly applicable to thermal contraction matching of external solvent to the protein lattice. Cryoprotectant exclusion from hydration layers and perturbation of water structure by protein surfaces complicates contraction matching of solvent in internal spaces, at least in lower-solvent-content crystals where the fraction of bulk-like solvent is small. Systematic study of, e.g., 298 K and 100 K mosaicity and cell parameters versus cryoprotectant concentration and versus the fraction of crystal solvent located in hydration shells may illuminate differences between internal and bulk solvent composition and structure.

### **Figure Captions**

**Figure 1** Experimental apparatus and protocol for determining the density of aqueous cryoprotectant drops. (a) Preparation of a dense liquid N<sub>2</sub>-Ar solution. (b) Cooling a drop of aqueous cryoprotectant mixture in the N<sub>2</sub>-Ar solution. (c) Visual observation of the drop's condition – clear or opaque/milky, uncracked or cracked, and whether it has positive, negative, or neutral buoyancy. (d) Determining the

density of the liquid N<sub>2</sub>-Ar solution that gives near neutral buoyancy of the drop. See Sections 2.2-2.6 for a detailed discussion.

**Figure 2** Measured density versus cryoprotectant concentration in % (w/w) at 77 K and literature values (Bosart & Snoddy, 1928; Rodrigues & Francesconi, 2011) at 298 K for (a) glycerol and (b) ethylene glycol. The solid and dashed lines are fits given by Equations 8 and 9, and with parameters as given in Table **S1**.

**Figure 3** Excess specific volume  $v^E = v_{actual} - v_{ideal}$  versus cryoprotectant concentration in % (w/w) at 77 K and 298 K for (a) glycerol and (b) ethylene glycol, calculated using Equations 5 and 6 and the densities in Figure 2. The solid lines are fits given by Eq. 8, with parameters as given in Table **S1**.

**Figure 4** Change in density between 298 K and 77 K vs. cryoprotectant concentration in % (w/w) for aqueous glycerol and ethylene glycol solutions. Data points are given by the difference between data points at 77 K and a fit to the measured (and more accurate) 298 K values. Fits are given by the difference between the fits to the 77 K and 298 K data in Figure 2.

**Figure 5** Specific volume v versus cryoprotectant concentration in % (w/w) for glycerol and ethylene glycol at 77 K. The black dotted lines give the ideal specific volume  $v_{ideal}$  (described by Eq. 6). The difference between the black dotted lines and each curve represents the excess specific volume  $v^E$ . The dashed lines indicate low- and high concentration asymptotes, corresponding to regions where the tetrahedral hydrogen bond network of LDA ice and the disordered hydrogen bond network of the pure amorphous cryoprotectant dominate, respectively.

**Figure 6** Apparent specific volumes of (a) cryoprotectant  $V_{cryo}^{app}\left(c_{\%w/w}\right)$  calculated using Equation 10 and (b) water  $V_{water}^{app}\left(c_{\%w/w}\right)$  calculated using Equation 11 vs. cryoprotectant concentration in % (w/w) for ethylene glycol and glycerol in water at 77 K.

**Acknowledgements** This work was supported by the NSF under award MCB-1330685.

#### **References Cited**

Alcorn, T. & Juers, D. H. (2010). Acta Crystallogr. Sect. D. 66, 366–373.

Berejnov, V., Husseini, N. S., Alsaied, O. A., & Thorne, R. E. (2006). *J. Appl. Crystallogr.* **39**, 244–251.

Blazhnov, I. V., Malomuzh, N. P., & Lishchuk, S. V. (2004). J. Chem. Phys. 121, 6435–6441.

Bosart, L. W. & Snoddy, A. O. (1928). Ind. Eng. Chem. 20, 1377–1379.

Bowron, D. T., Finney, J. L., Hallbrucker, A., Kohl, I., Loerting, T., Mayer, E., & Soper, A. K. (2006). *J. Chem. Phys.* **125**, 1–14.

Caylor, C. L., Dobrianov, I., Lemay, S. G., Kimmer, C., Kriminski, S., Finkelstein, K. D., Zipfel, W., Webb, W. W., Thomas, B. R., Chernov, a a, et al. (1999). *Proteins*. **36**, 270–281.

Charron, C., Kadri, A., Robert, M., Giege, R., & Lorber, B. (2002). *Acta Crystallogr. Sect. D.* **58**, 2060–2065.

Chinte, U., Shah, B., DeWitt, K., Kirschbaum, K., Pinkerton, A. A., & Schall, C. (2005). *J. Appl. Crystallogr.* 38, 412–419.

Datta, S., Biswal, B. K., & Vijayan, M. (2001). Acta Crystallogr. Sect. D. 57, 1614–1620.

Debenedetti, P. G. (2003). J. Phys. Condens. Matter. 25, 351-R1726.

Egorov, G. I. & Makarov, D. M. (2014). J. Chem. Thermodyn. 79, 135–158.

Egorov, G. I., Makarov, D. M., & Kolker, A. M. (2010). Russ. J. Gen. Chem. 80, 1577-1585.

Fourme, R., Ducruix, A., Ries-Kautt, M., & Capelle, B. (1995). J. Synchrotron Radiat. 2, 136–142.

Garman, E. (1999). Acta Crystallogr. Sect. D. 55, 1641–1653.

Garman, E. F. (2010). Acta Crystallogr. Sect. D. 66, 339–351.

Garman, E. F. & Doublié, S. (2003). Methods Enzymol. 368, 188-216.

Garman, E. F. & Mitchell, E. P. (1996). J. Appl. Crystallogr. 29, 584–587.

Garman, E. F. & Schneider, T. R. (1997). J. Appl. Crystallogr. 30, 211–237.

Ghormley, A. J. & Hochanadel, C. J. (1971). Science (80-.). 171, 62–64.

Halle, B. (2004). Proc. Natl. Acad. Sci. 101, 4793–4798.

Holton, J. M. (2009). J. Synchrotron Radiat. 16, 133-142.

Juers, D. H. & Matthews, B. W. (2001). J. Mol. Biol. 311, 851–862.

Juers, D. H. & Matthews, B. W. (2004a). Q. Rev. Biophys. 37, 105–119.

Juers, D. H. & Matthews, B. W. (2004b). Acta Crystallogr. Sect. D. 60, 412–421.

Keedy, D. A., van den Bedem, H., Sivak, D. A., Petsko, G. A., Ringe, D., Wilson, M. A., & Fraser, J. S. (2014). *Structure*. **22**, 1–12.

Keedy, D. A., Kenner, L. R., Warkentin, M., Woldeyes, R. A., Hopkins, J. B., Thompson, M. C., Brewster, A. S., Benschoten, A. H. Van, Baxter, E. L., Uervirojnangkoorn, M., et al. (2015). *Elife*. 07574.

Kmetko, J., Husseini, N. S., Naides, M., Kalinin, Y., & Thorne, R. E. (2006). *Acta Crystallogr. Sect. D.* **62**, 1030–1038.

Kriminski, S., Caylor, C. L., Nonato, M. C., Finkelstein, K. D., & Thorne, R. E. (2002). *Acta Crystallogr. Sect. D.* **58**, 459–471.

Loerting, T., Bauer, M., Kohl, I., Watschinger, K., Winkel, K., & Mayer, E. (2011). *J. Phys. Chem. B.* **115**, 14167–14175.

Malkin, A. J. & Thorne, R. E. (2004). *Methods*. **34**, 273–299.

McFerrin, M. B. & Snell, E. H. (2002). J. Appl. Crystallogr. 35, 538-545.

Meisburger, S. P., Warkentin, M., Chen, H., Hopkins, J. B., Gillilan, R. E., Pollack, L., & Thorne, R. E. (2013). *Biophys. J.* **104**, 227–236.

Merzel, F. & Smith, J. C. (2002). Proc. Natl. Acad. Sci. U. S. A. 99, 5378-5383.

Parsegian, V. A., Rand, R. P., & Rau, D. C. (2000). Proc. Natl. Acad. Sci. U. S. A. 97, 3987–3992.

Pflugrath, J. W. (2015). Acta Crystallogr. Sect. F. 71, 622–642.

Rodrigues, M. & Francesconi, A. Z. (2011). J. Solution Chem. 40, 1863–1873.

Röttger, K., Endriss, A., Ihringer, J., Doyle, S., & Kuhs, W. F. (1994). *Acta Crystallogr. Sect. B.* **50**, 644–648.

Saraswathi, N. T., Sankaranarayanan, R., & Vijayan, M. (2002). *Acta Crystallogr. Sect. D.* **58**, 1162–1167.

Shimizu, S. & Smith, D. J. (2004). J. Chem. Phys. 121, 1148-1154.

Sinibaldi, R., Ortore, M. G., Spinozzi, F., Carsughi, F., Frielinghaus, H., Cinelli, S., Onori, G., & Mariani, P. (2007). *J. Chem. Phys.* **126**, 235101.

Snell, E. H., Weisgerber, S., Helliwell, J. R., Weckert, E., Holzer, K., & Schroer, K. (1995). *Acta Crystallogr. Sect. D Biol. Crystallogr.* **51**, 1099–1102.

Sutton, R. L. (1991a). J. Chem. Soc. Faraday Trans. 87, 3747–3751.

Sutton, R. L. (1991b). J. Chem. Soc. Faraday Trans. 87, 101–105.

Timasheff, S. N. (1993). Annu. Rev. Biophys. Biomol. Struct. 22, 67–97.

Timasheff, S. N. (2002). *Biochemistry*. 41, 13473–13482.

Vekilov, P. G., Thomas, B. R., Stojanoff, V., & Rosenberger, F. (1996). *Acta Crystallogr. Sect. D.* **52**, 785–798.

Warkentin, M., Berejnov, V., Husseini, N. S., & Thorne, R. E. (2006). J. Appl. Crystallogr. 39, 805–811.

Warkentin, M., Hopkins, J. B., Badeau, R., Mulichak, A. M., Keefe, L. J., & Thorne, R. E. (2013a). *J. Synchrotron Radiat.* **20**, 7–13.

Warkentin, M., Sethna, J., & Thorne, R. (2013b). Phys. Rev. Lett. 110, 015703.

# **Supporting information**

**Table S1** Parameters for the fits to the excess specific volume in Figure 3 and S2 given by Equation 8, obtained by nonlinear regression, and for fits to the density in Figure 2 given by Equation 9.

Parameter	Glycerol		Ethylene Glycol	
	298 K	77 K	298 K	77 K
$a_0$	-0.0164	-0.118	-0.0236	-0.114
$a_1$	53.01	49.39	52.89	49.14
a <sub>2</sub>	40.18	39.49	44.28	37.91
a <sub>3</sub>	0.00695	0.0541	0.0127	0.0489

# **Figure Captions**

**Figure S1** Measured density versus cryoprotectant concentration in % (w/v) at 77 K and literature values (Bosart & Snoddy, 1928; Rodrigues & Francesconi, 2011) at 298 K for (a) glycerol and (b) ethylene glycol. The solid and dashed lines are fits given by Equations 8 and 9, and with parameters as given in Table **S1**.

**Figure S2** Excess specific volume  $v^E = v_{actual} - v_{ideal}$  versus cryoprotectant concentration in % (w/v) at 77 K and 298 K for (a) glycerol and (b) ethylene glycol, calculated using Equations 5 and 6 and the densities in Figure 2. The solid lines are fits given by Eq. 8, with parameters as given in Table S1.

**Figure S3** Change in density between 298 K and 77 K vs. cryoprotectant concentration in % (w/v) for aqueous glycerol and ethylene glycol solutions. Data points are given by the difference between data points at 77 K and a fit to the measured (and more accurate) 298 K values. Fits are given by the difference between the fits to the 77 K and 298 K data in Figure 2.

**Figure S4** Apparent specific volumes of water calculated using Equation 11 vs. cryoprotectant concentration in % (w/w) for ethylene glycol and glycerol in water at 298 K.

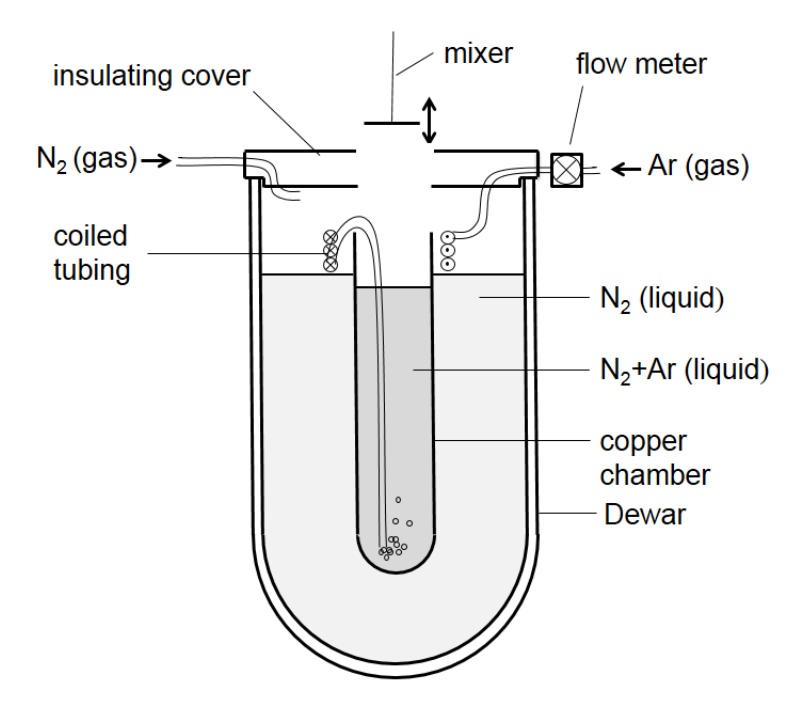


Figure 1(a)

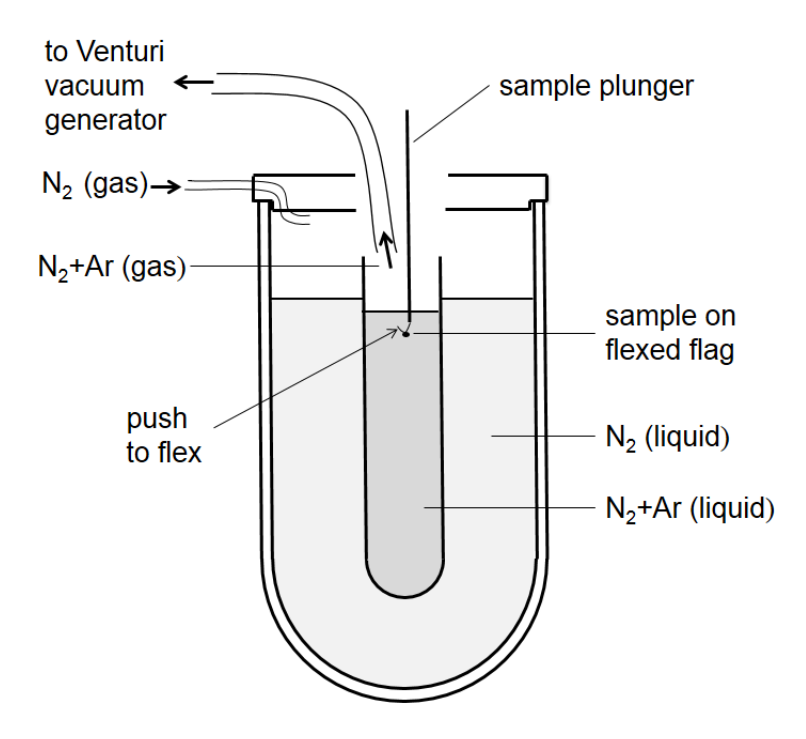


Figure 1(b)

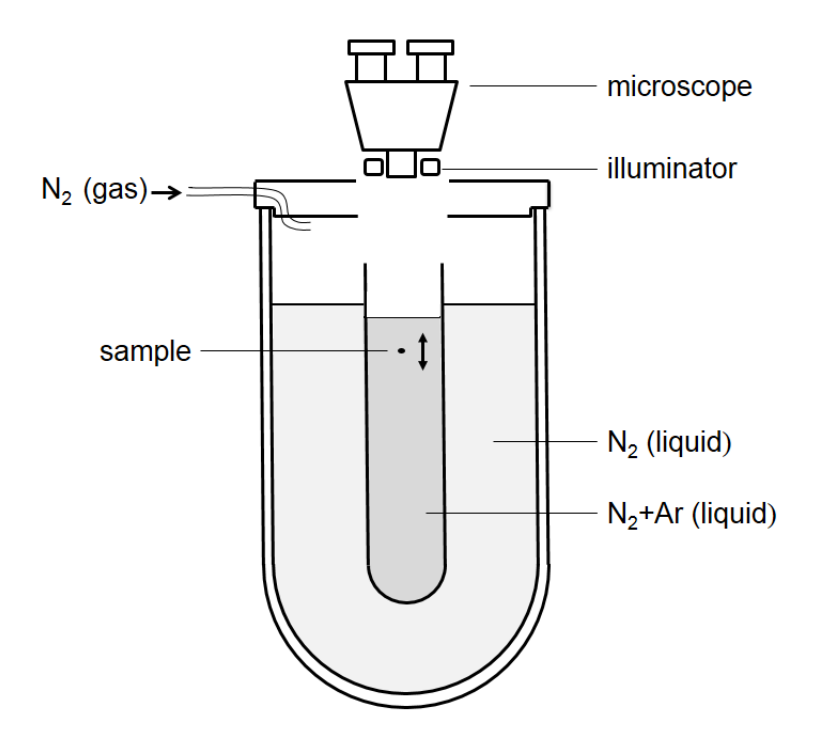


Figure 1(c)

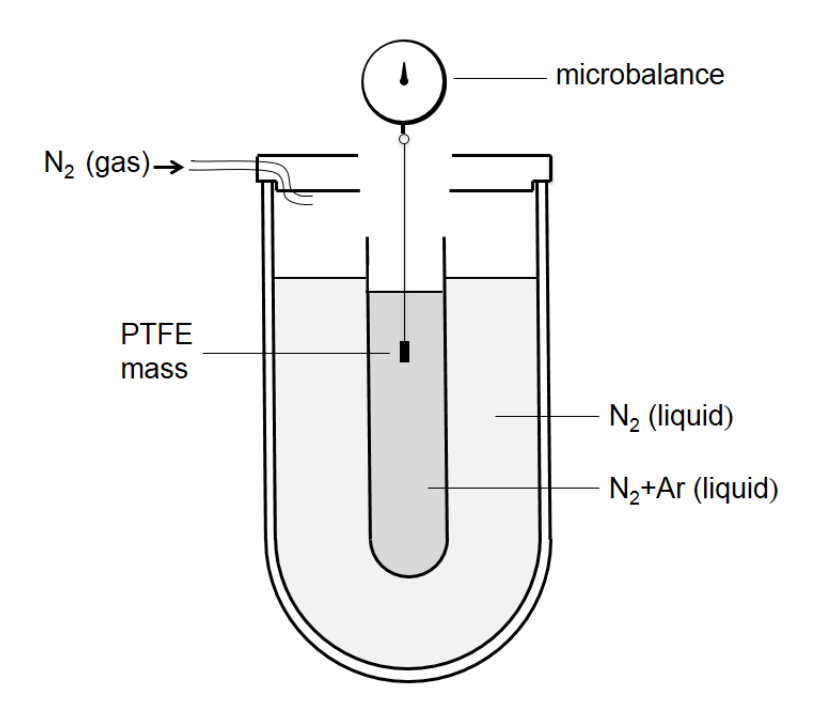


Figure 1(d)

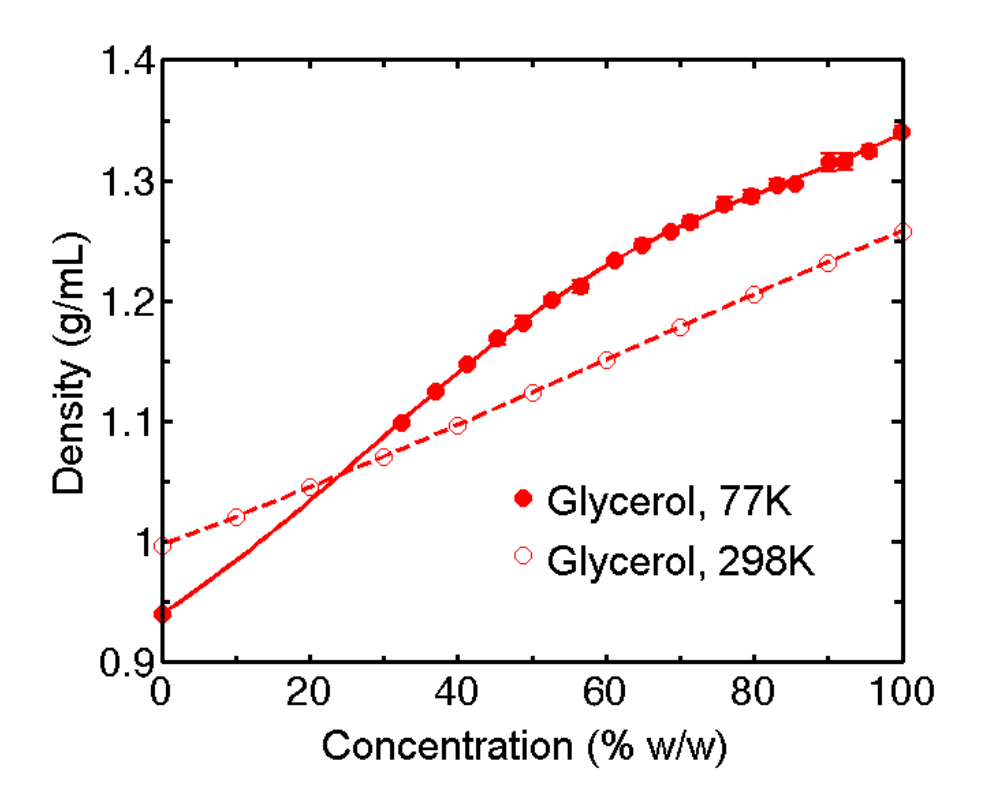


Figure 2(a)

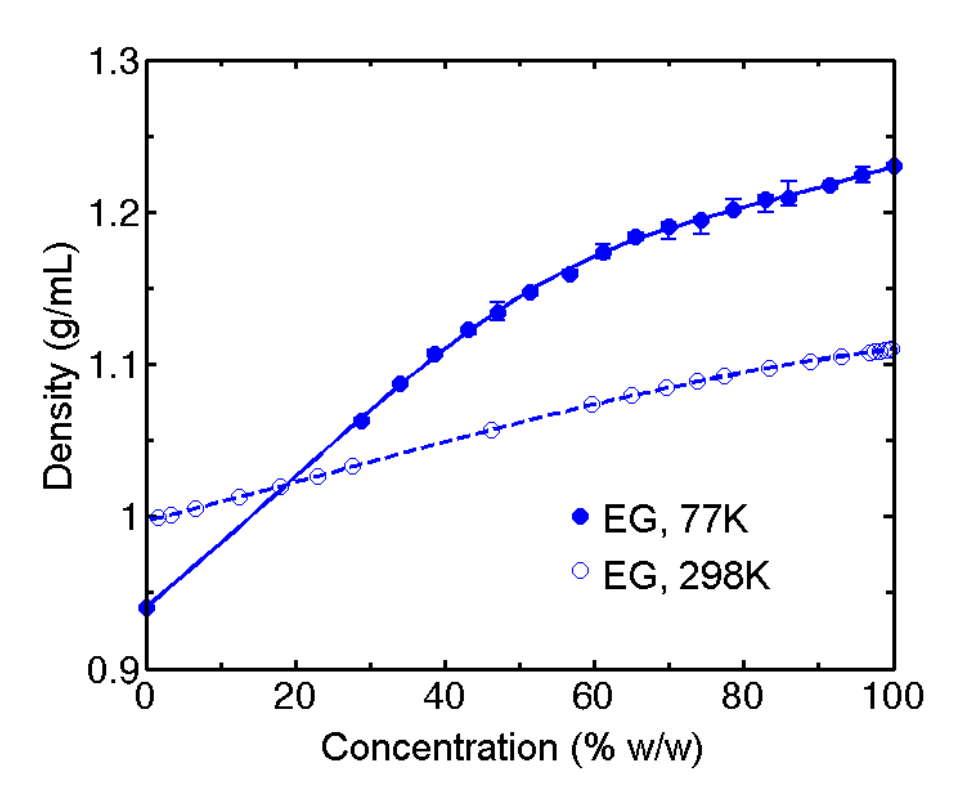


Figure 2(b)

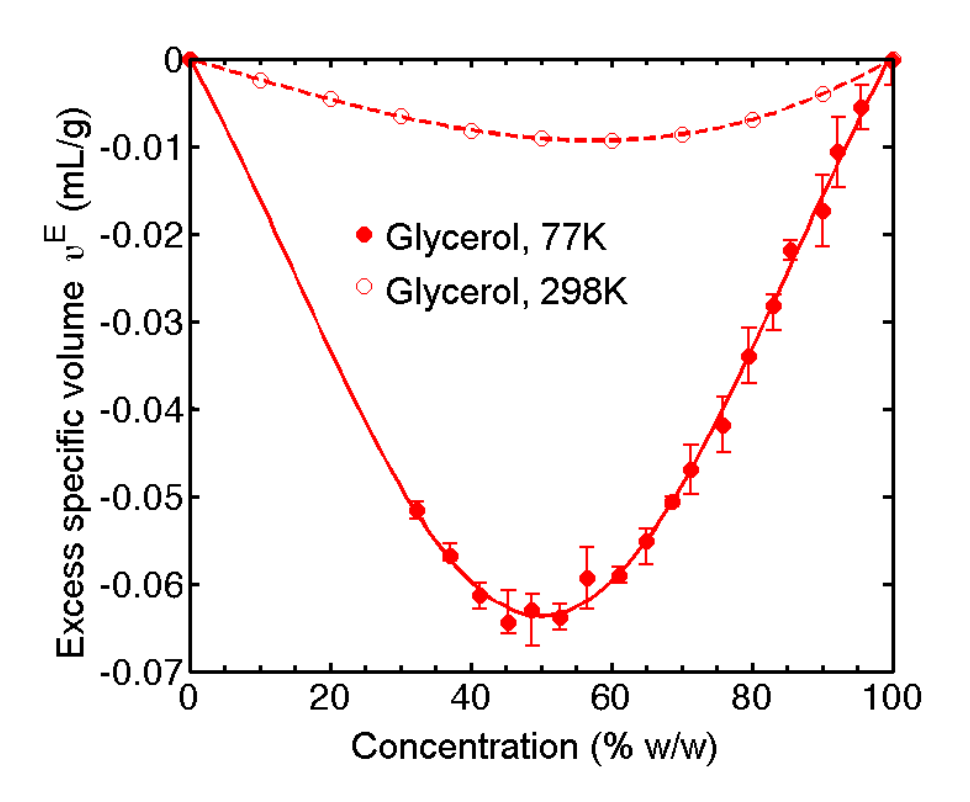


Figure 3(a)

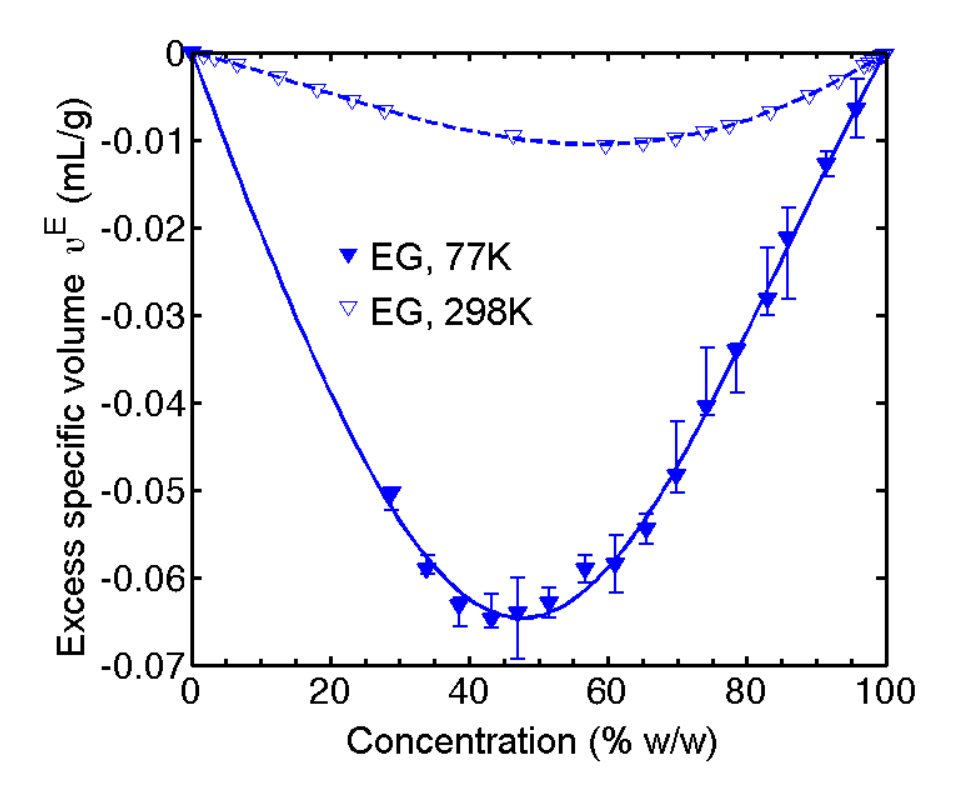


Figure 3(b)

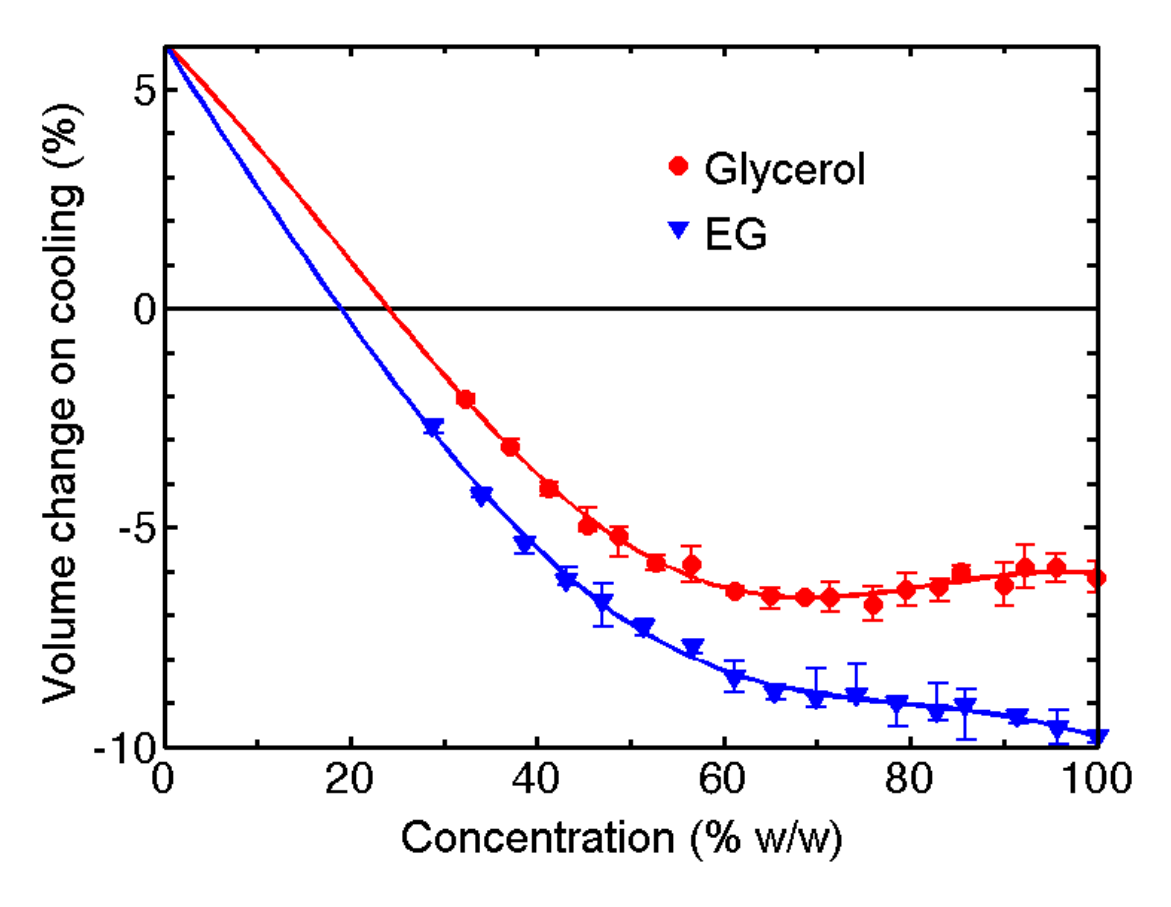


Figure 4

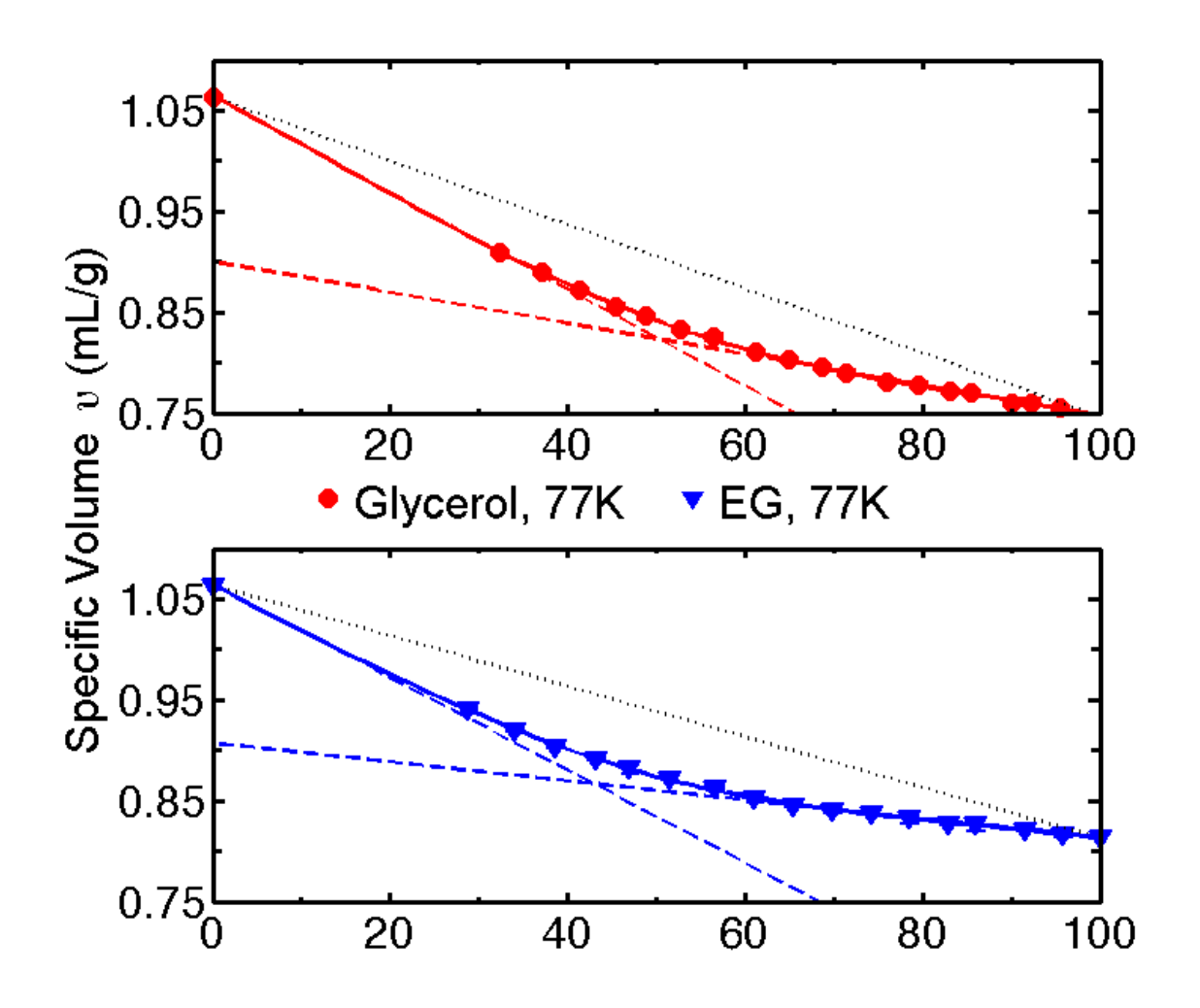


Figure 5

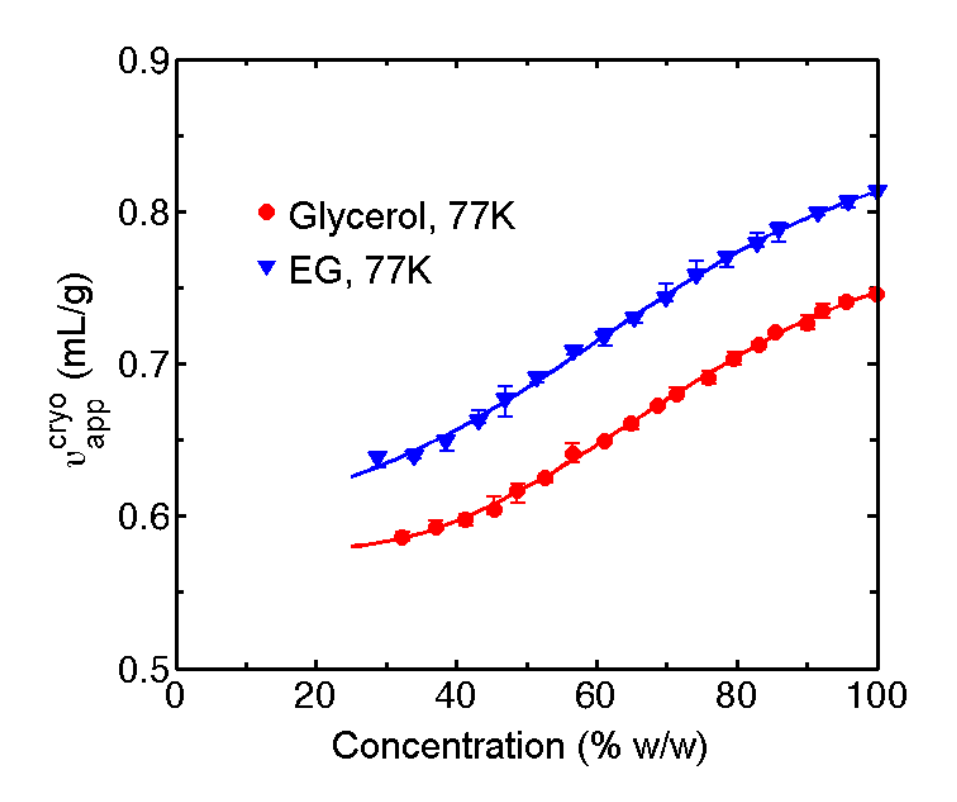


Figure 6(a)

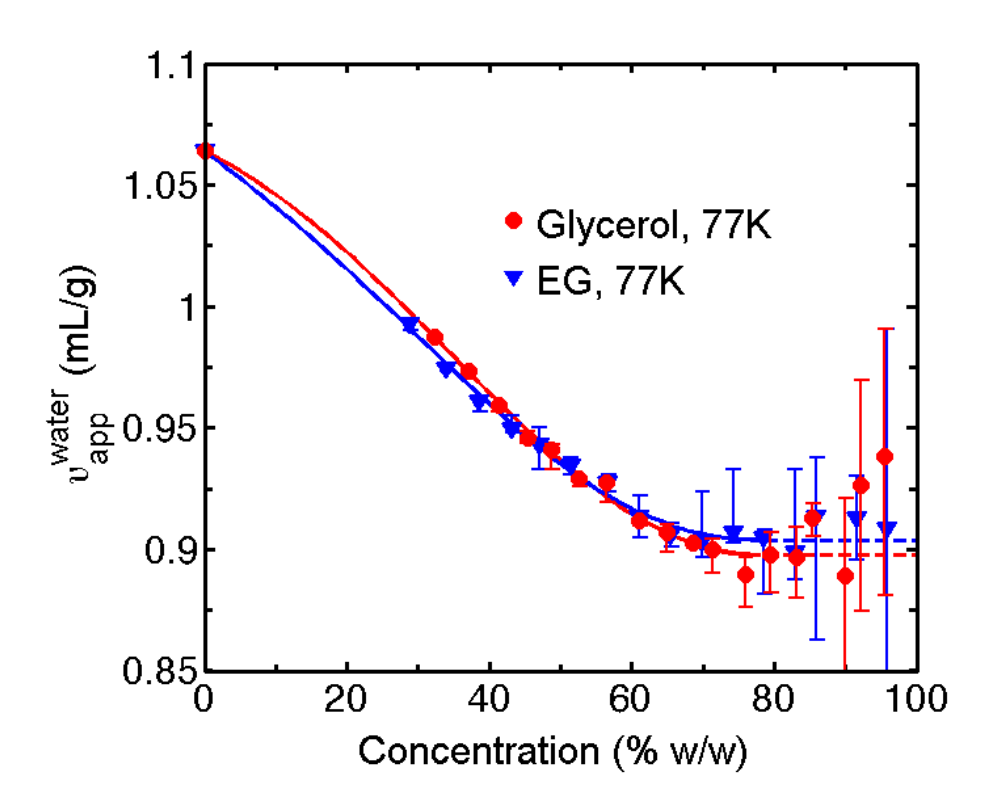


Figure 6(b)

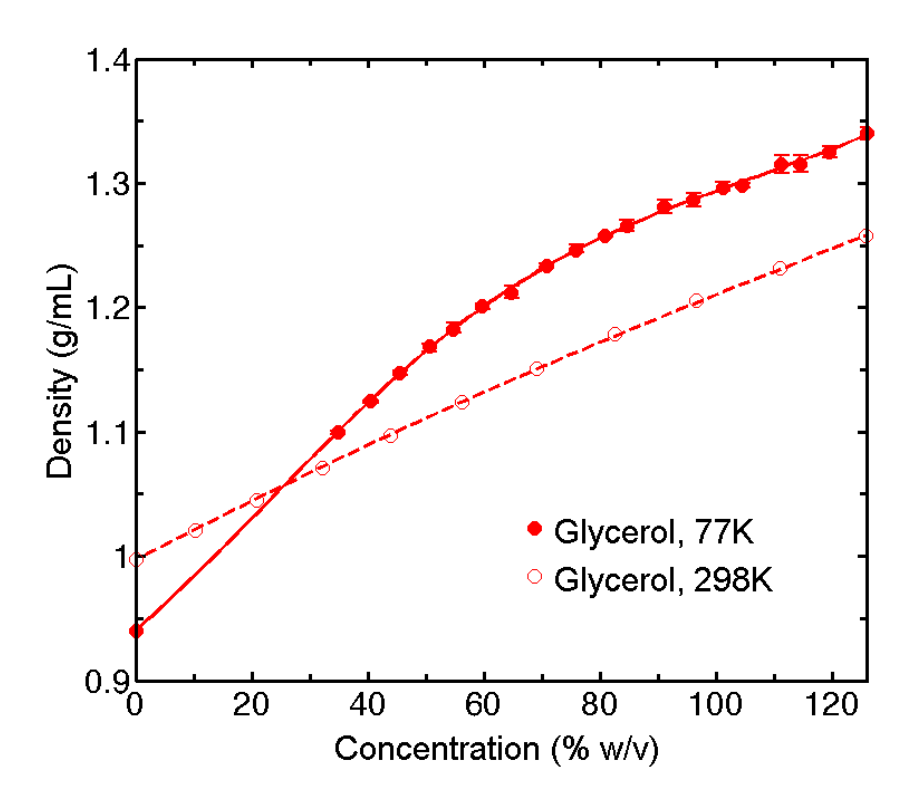


Figure S1(a)

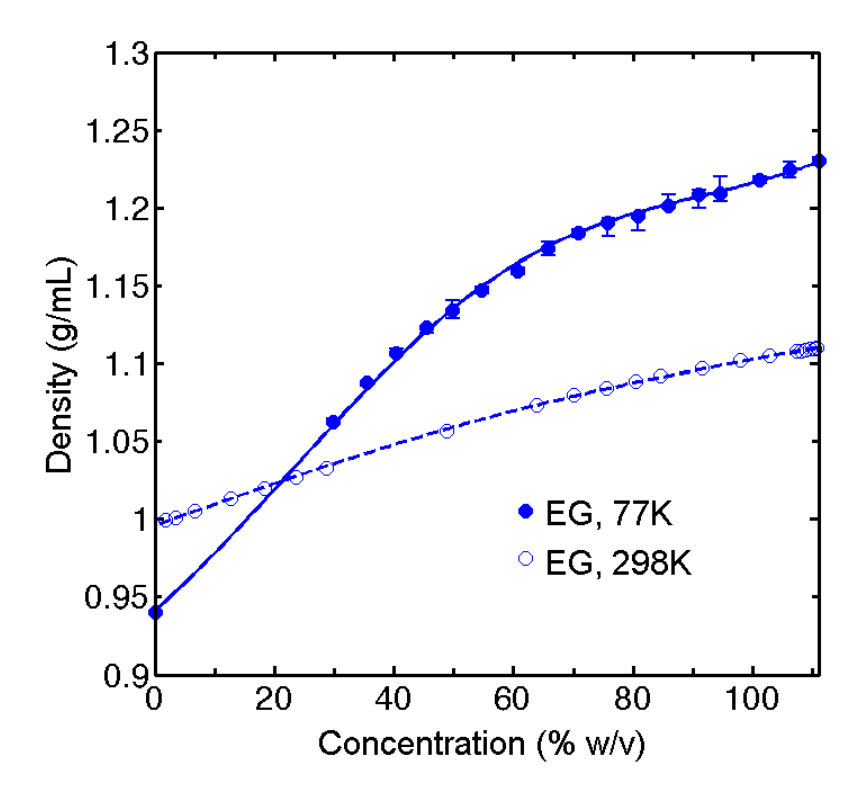


Figure S1(b)

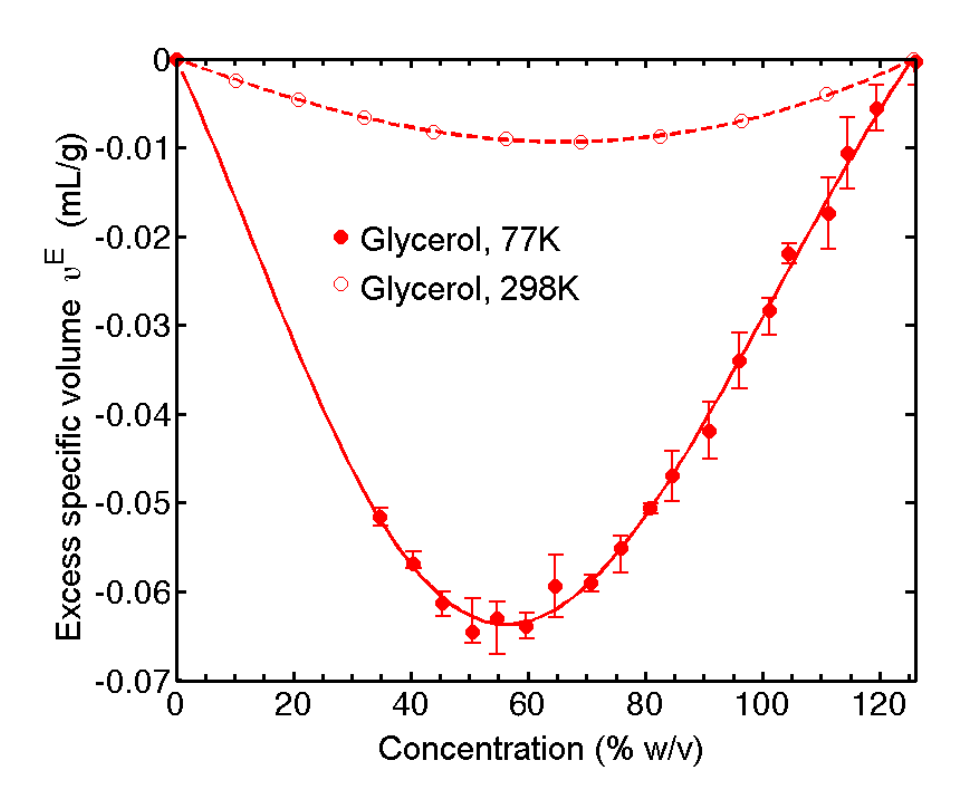


Figure S2(a)

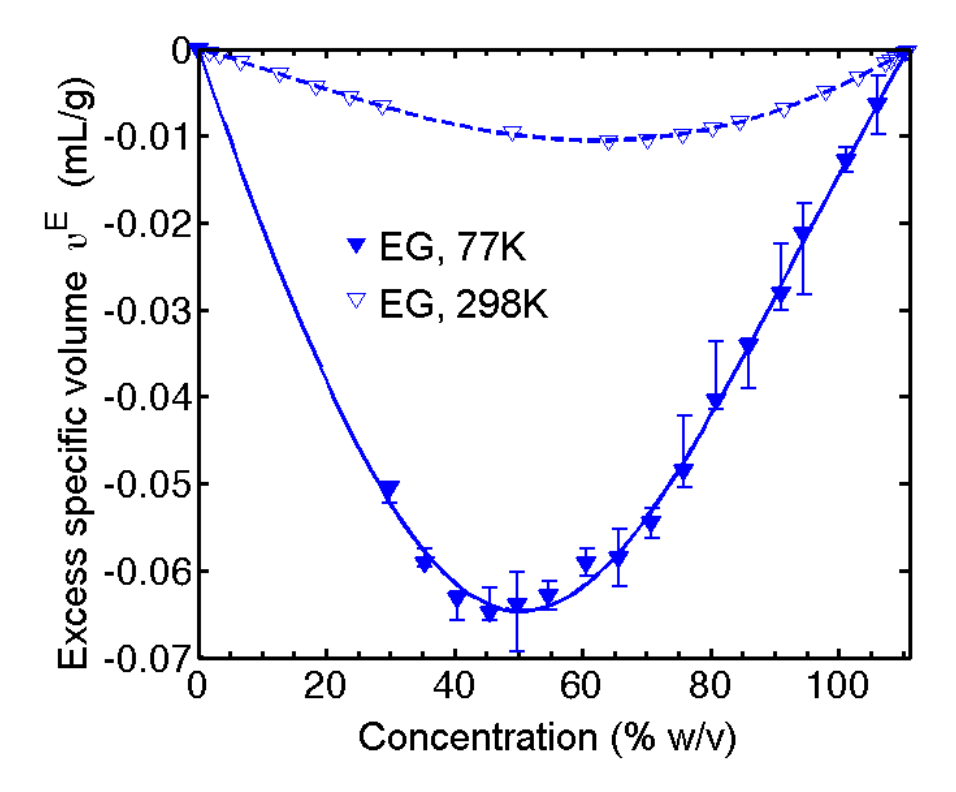


Figure S2(b)

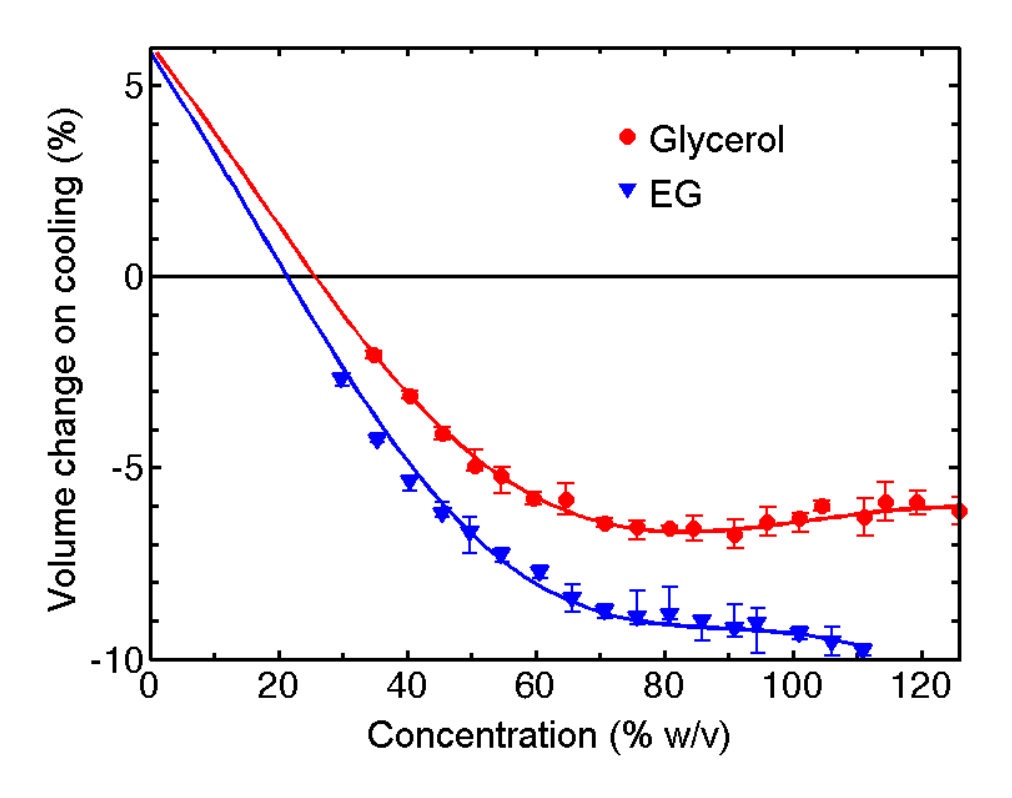


Figure S3

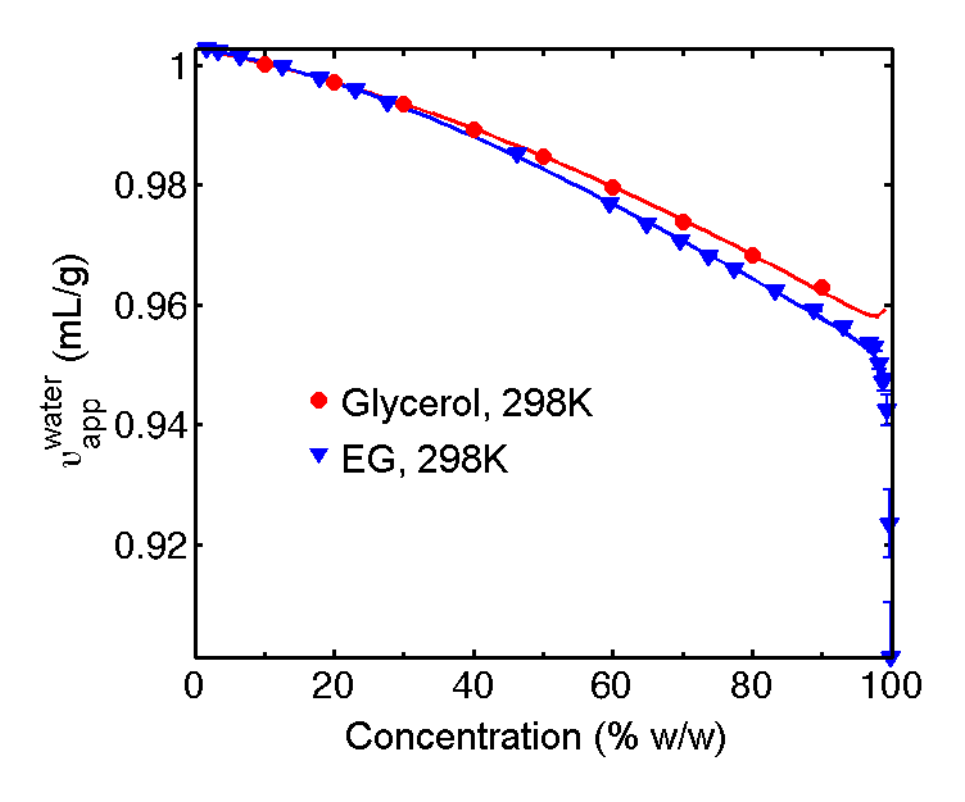


Figure S4